https://www.overleaf.com/project/62d1140fd68c9d599f15469e

Stress relaxation of AlGaN on nonpolar m-plane GaN substrate

Yingying Lin,[1] Hadi Sena,[2] Martin Frentrup,[3] Markus Pristovsek,[2] Yoshio Honda,[2] and Hiroshi Amano[2]
[1)]*Graduate School of Engineering, Nagoya University, Chikusa-Ku, Furo-cho, Nagoya 464-8603, Japan*
[2)]*Center for Integrated Research of Future Electronics, Institute for Materials and Systems for Sustainability, Nagoya University, Chikusa-Ku, Furo-cho, Nagoya 464-8603, Japan*
[3)]*Cambridge Centre for Gallium Nitride, Department of Materials Science and Metallurgy, University of Cambridge, 27 Charles Babbage Road, Cambridge CB3 0FS, United Kingdom*

(*Electronic mail: lin.yinging.e2@s.mail.nagoya-u.ac.jp)

The stress relaxation with increasing thickness of metal-organic vapour phase epitaxy (MOVPE) grown $Al_{0.19}Ga_{0.81}N$ on quasi-bulk $(10\bar{1}0)$ m-plane GaN substrates was investigated by X-ray diffraction. The anisotropic in-plane stress leads to an orthorhombic distortion of the lattice, which requires special mathematical treatment. Extending earlier works, we developed a method to calculate the distortion along $[1\bar{2}10]$, [0001] and $[10\bar{1}0]$ and get the lattice parameters, Al content, and strain values. The stress relaxation along the two in-plane directions involves two different mechanisms. First, the stress along $[1\bar{2}10]$ relaxes by the onset of misfit dislocations through the $\{10\bar{1}0\}\langle 1\bar{2}10\rangle$ slip system while for thicker layers the stress along [0001] relaxes by crack formation. Comparing the cathodoluminescense emission at room temperature with the expected bandgap showed that both tensile in-plane strains along $[1\bar{2}10]$ and [0001] decrease the band gap.

I. INTRODUCTION

III-Nitrides have historically received attention mostly for electronic and optoelectronics applications. The most common growth orientation for III-nitrides in the wurtzite crystal structures is along [0001], the c-axis. However, considerable efforts have been put into nonpolar and semipolar III-nitride orientations allowing to reduce the polarization-induced fields across heterostructures. However, ternary alloys AlGaN and InGaN are often grown heteroepitaxially on foreign substrates, which leads to anisotropic in-plane stress. For example, the lattice mismatch of $(10\bar{1}0)$ AlN on bulk GaN is -0.024 in *a* direction and -0.04 in *c* direction. When the thickness of a mismatched layer exceeds a critical thickness, stress relaxation occurs. For many materials, stress relaxation occurs through the formation of the misfit dislocations (MDs) by the glide along a slip system. However, the common (0001) plane does not possess a suitable slip system, while semi- and non-polar GaN have one or more (e.g.[1] for $(11\bar{2}2)$ orientation). Moreover, the elastic properties differ along *a* $[1\bar{2}10]$, *c* [0001], and *m* $[10\bar{1}0]$ directions. Thus, the orientation has a severe impact on the stress and relaxation mechanism[2].

For the AlGaN on (0001) GaN the tensile stress leads to cracking when a certain surface energy has accumulated[3,4], although some glide can occur via secondary slip systems[5]. The stress relaxation could also be affected by dislocations (as shown for InGaN[6]), or by anisotropic stress field, e.g. from patterned growth[7].

For non-polar AlGaN on $(10\bar{1}0)$ GaN, the anisotropic lattice and thermal mismatches lead to different stress on the surface in [0001] and $[1\bar{2}10]$ directions, and glide is possible. This leads to an anisotropic distortion of the hexagonal lattice cell[8], which makes X-ray characterization more challenging, and affects also the critical thicknesses[9].

In our study, we grew $Al_{0.19}Ga_{0.81}N$ layers with different thicknesses on $(10\bar{1}0)$ GaN quasi-bulk and investigated the lattice deformation and stress relaxation mechanism. From this, we could obtain the band gap shift due to strains along both $[1\bar{2}10]$ and [0001], which has never been done before and can provide important data for comparison with density functional theory (DFT) calculation.

II. EXPERIMENTAL

The substrates were hydride vapour phase epitaxy (HVPE) grown quasi-bulk GaN from Mitsubishi Chemicals with an offcut of 0.5° to a-direction to suppress spiral growth induced formation of hillocks[10].

All AlGaN layers have been grown in a horizontal 1x2" high temperature (TaC coated inner part) metal-organic vapor phase epitaxy reactor from EpiQuest. After loading the quasi-bulk $(10\bar{1}0)$ GaN substrates, they were heated up to 1000 °C (thermocouple), and a GaN buffer layer was grown for 30 minutes with a V/III ratio of 500 under hydrogen.

For the growth of AlGaN layer, the temperature was raised to 1080 °C with a TMGa partial pressure of 3.2 Pa, a TMAl dimers partial pressure of 0.9 Pa, and a V/III ratio of 500. After growth, the sample was cooled to room temperature immediately under NH_3 and H_2 ambient.

For the structural characterisation by high-resolution X-ray diffraction (XRD), reciprocal space maps (RSMs) of 5 symmetric and asymmetric reflections were measured with a PANalytical PIXcel detector in either an Empyrean or an X'pert MRD PRO diffractometer.

A coarse characterisation of the surface was obtained using white light holography and selected samples were measured with a Hitachi atomic force microscope (AFM).

The thickness was estimated from the XRD diffraction fringes of the symmetric $10\bar{1}0$ and $30\bar{3}0$ reflection for thin layers, from interference fringes using vertical deep UV light

reflection, and from cross-sections in scanning electron microscopy (SEM).

III. SURFACE AND XRD MEASUREMENTS

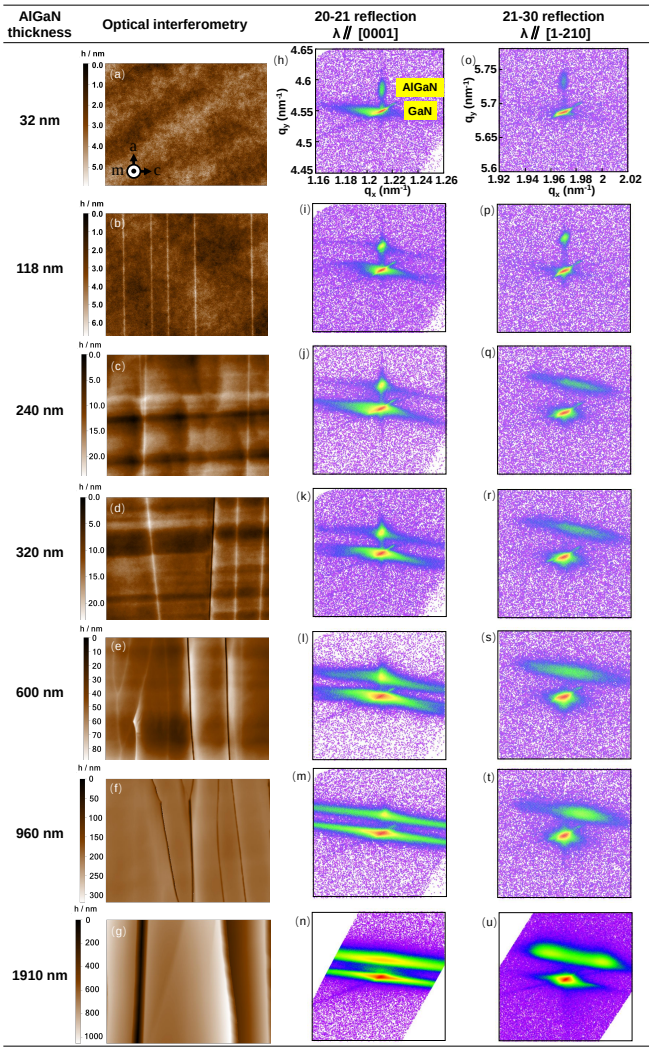


FIG. 1. (a)-(g) White light interference topography of the surface of AlGaN with different thicknesses on m-plane GaN. The size of the surface area is the same of 31 μm×42 μm. Reciprocal space map (RSM) of (h)-(n) the $20\bar{2}1$ and (o)-(u) $21\bar{3}0$ asymmetric reflection at different thicknesses of AlGaN. Each of the $20\bar{2}1$ RSMs and $21\bar{3}0$ RSMs span the same area given in the first row.

Fig. 1 left column shows the surface topography measured by optical interferometry. The surface after growth of 32 nm AlGaN (Fig. 1a) was identical to the initial GaN surface. It was flat without any pits or hillocks. For thicknesses of 118 nm and more, ridges (white stripes) appeared which run mostly parallel to $[1\bar{2}10]$. At 240 nm and 320 nm AlGaN the surface showed additional broad nearly rectangular valleys along [0001]. Finally, the first cracks along $[1\bar{2}10]$ appear at 320 nm AlGaN. With the increasing AlGaN thickness, the cracks get denser and wide and increase the surface height undulation. However, the cracks only appeared in $[1\bar{2}10]$ direction, which is very different from the [0001] direction.

Fig. 2a shows an AFM image of two ridges with their cross-section after 118 nm AlGaN growth. The ridges protrude 2-3 nm above the surface. Since the ridges run along $[1\bar{2}10]$ direction, one might assume these are connected to stacking faults. However, as one can see in Fig. 1, the ridges tend to slightly tilt with respect to $[1\bar{2}10]$ with increasing AlGaN thickness and show even branching, which cannot occur with stacking faults. Therefore, the ridges are more likely related to the domain structure of the m-GaN substrates, which is enhanced by the stress.

Fig. 2b shows the surface after 960 nm AlGaN growth, which shows the severe cracks together with a strong undulation perpendicular to them. The undulation is possibly related to the remaining incompletely relieved tensile stress. The observed cracks are roughly parallel to $[1\bar{2}10]$ but with some inclination, likely due to residual stress due to the use of misoriented substrates and the stress after HVPE growth and wafering.

To investigate the strain state and Al content of the AlGaN layers, asymmetric RSMs of the $20\bar{2}1$ and $21\bar{3}0$ reflections were measured (Fig. 1). For these two reflections, the X-ray beam is coplanar with the [0001] in-plane direction for the $20\bar{2}1$ reflection and coplanar with $[1\bar{2}10]$ for the $21\bar{3}0$ reflection, which allows for a quick visual interpretation of the relaxation along both in-plane directions.

For the $20\bar{2}1$ reflection, the AlGaN layer reflection is centered above the GaN reflection for thin AlGaN layers up to a thickness of 600 nm and just broadens with increasing thickness. Only for 960 nm and 1910 nm AlGaN maximum position deviate in q_x from the GaN position indicating a partial relaxation in this direction, while already for 240 nm thick AlGaN an offset in q_x appears for the $21\bar{3}0$ reflection connected with strong broadening.

After 1910 nm, a second AlGaN maxima appear on the $21\bar{3}0$ reflection, which indicates a macroscopic tilt of the AlGaN crystal lattice along $[1\bar{2}10]$ direction. This phenomenon has been reported before for m-plane InGaN/GaN and results from the glide of either $(01\bar{1}0)$ or $(1\bar{1}00)$ planes of the $\langle 1\bar{2}10\rangle$ slip systems[9,11,12]. In the slip system of $\{10\bar{1}0\}\langle 1\bar{2}10\rangle$, the slip plane of $(0\bar{1}10)$ or $(1\bar{1}00)$ can glide either $\pm 60^\circ$ along $[\bar{2}110]$ or $[\bar{1}2\bar{1}0]$. Thus, two symmetrical separated lattice tilts were produced.

Different from InGaN on GaN[11], we observed the splitting of the $21\bar{3}0$ reflection on the AlGaN/GaN heterostructure only at much higher thicknesses. The different tendencies in RSMs along [0001] and $[1\bar{2}10]$ with increasing thicknesses indicate the different ways of relaxation for in-plane [0001] and $[1\bar{2}10]$ directions on m-plane.

IV. CALCULATING THE RELAXATION

First, one has to obtain the lattice constants and from those the Al-content to finally get the strain. This has been done for non-polar III-nitrides by Laskar et al.[8]. They described the or-

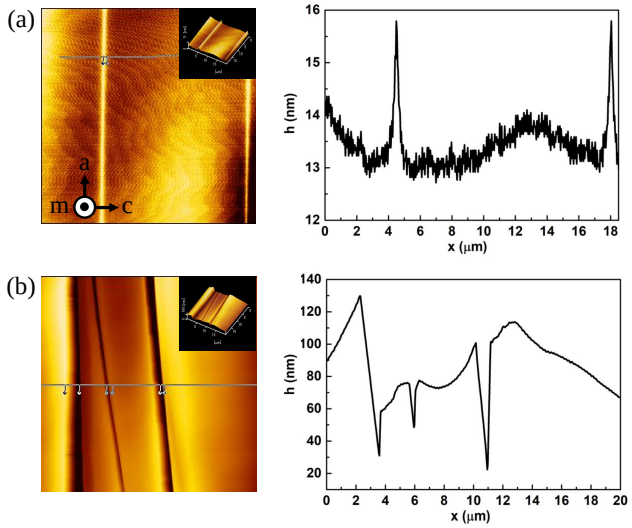


FIG. 2. Atomic force microscopy images, with corresponding line-cuts in topography obtained from (a) 118 nm (top row) and (b) 960 nm (bottom row) AlGaN films.

thorhombic distortion by an angular deviation from the 120° symmetry within the basal plane. However, the use of an angle as a third parameter makes the formulas more complicated than necessary. Therefore, we modified the method of Frentrup et al.[13] to a relatively simple procedure. Both methods require the measurement of the 2θ angles of several symmetric and asymmetric reflections, at least three for exact $(10\bar{1}0)$ orientation. (We ignore the offcut angle of 0.5° which would in principle need to consider the shear stress, like in the full semipolar calculation[13].)

A. Obtaining the lattice constants

For any reciprocal lattice vector $\boldsymbol{g} = h\boldsymbol{a}^* + k\boldsymbol{b}^* + l\boldsymbol{c}^*$, it is normal to the (hkl)-plane and its magnitude equal to the reciprocal of the inter-planar spacing of the (hkl)-planes. The inter-planar lattice distance d of hkl planes for the general unit cell can be calculated by three lattice parameters a, b, c and three angles α, β, γ:

$$\frac{1}{d_{hkl}^2} = \frac{1}{V^2}(S_{11}h^2 + S_{22}k^2 + S_{33}l^2 + 2S_{12}hk + 2S_{23}kl + 2S_{13}hl), \tag{1}$$

with volume V and S_{ij} given by:

$$V = abc(1 - \cos^2\alpha - \cos^2\beta - \cos^2\gamma + 2\cos\alpha\cos\beta\cos\gamma)^{\frac{1}{2}} \tag{2}$$

$$S_{11} = b^2c^2\sin^2\alpha$$
$$S_{22} = a^2c^2\sin^2\beta$$
$$S_{33} = a^2b^2\sin^2\gamma$$
$$S_{12} = abc^2(\cos\alpha\cos\beta - \cos\gamma)$$
$$S_{23} = a^2bc(\cos\beta\cos\gamma - \cos\alpha)$$
$$S_{13} = ab^2c(\cos\gamma\cos\alpha - \cos\beta).$$

For our case of $(10\bar{1}0)$ orientation, the anisotropic in-plane stress leads to the orthorhombic distortion still preserves the orthogonality of coordinates along $[1\bar{2}10]$, $[10\bar{1}0]$, [0001] (Fig. 3a). Therefore, we set the base angles to α=β=γ=90°, by which the inter-planar spacing of $h'k'l'$ planes in the orthorhombic system can be simplified as:

$$\frac{1}{d_{hkl}^2} = \frac{h'^2}{a^2} + \frac{k'^2}{b^2} + \frac{l'^2}{c^2}. \tag{3}$$

To transform the 4-digit Miller Bravais indices $hkil$ of the hexagonal lattice into a 3-digit system $h'k'l'$ of the orthorhombic lattice, the vectors have to be projected on the base vectors along $[1\bar{2}10]$, $[10\bar{1}0]$ and [0001]. Here we define the $[1\bar{2}10]$ as a-direction, $[10\bar{1}0]$ as m-direction, [0001] as c-direction. As shown in Fig. 3b, the reciprocal lattice vector $\boldsymbol{g}$ can be described in the form of vector $\boldsymbol{a}$, $\boldsymbol{m}$, $\boldsymbol{c}$ as:

$$\boldsymbol{g} = -k\boldsymbol{a} + (2h+k)\boldsymbol{m} + l\boldsymbol{c}. \tag{4}$$

Now the expression of the interplanar distance d_{hkl} can be written as:

$$\frac{1}{d_{hkl}^2} = \frac{k^2}{a^2} + \frac{(2h+k)^2}{m^2} + \frac{l^2}{c^2}. \tag{5}$$

Thus, eq. (5) connects the interplanar spacing with the unknown lattice constants:

$$\frac{1}{d_{hkl}^2} = [k^2]x_1 + [(2h+k)^2]x_2 + [l^2]x_3, \tag{6}$$

where the x_1=a^{-2}, x_2=m^{-2}, x_3=c^{-2}.

According to Bragg's law, the interplanar distance can be obtained from the Bragg angle by XRD measurement.

$$\frac{1}{d_\theta^2} = \left(\frac{2\sin\theta_{hkl}}{\lambda}\right)^2 \tag{7}$$

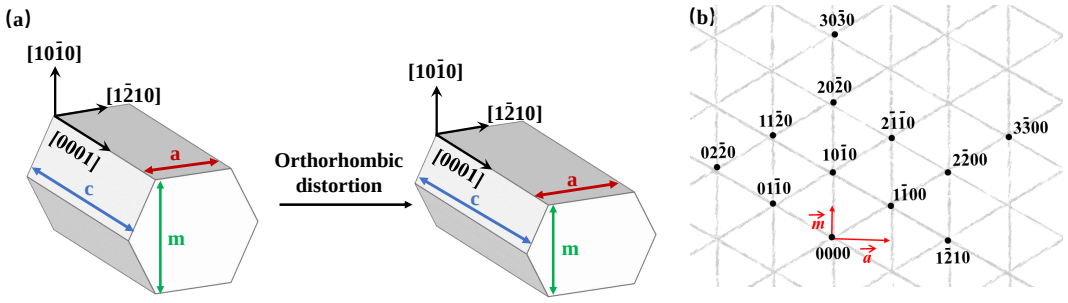


FIG. 3. (a) Schematic diagram showing the relative orientation and the corresponding lattice parameters of wurtzite unit cell of (10$\bar{1}$0) m-plane oriented III-nitride epilayer. The orthorhombic distortion on m-plane oriented crystals still preserves the orthogonality of coordinates along [1$\bar{2}$10], [10$\bar{1}$0] and [0001]. (b) illustration of the coordinate transformation of the basis vectors in the hexagonal reciprocal space lattice.

In the experiment we measured n independent reflection planes from $i = 1 \ldots n$ with indices $(h_i k_i l_i)$ and with the diffraction angle θ_i. We can combine the right sides of eq. (6) and (7) in a matrix equation:

$$\begin{pmatrix} \left(\frac{2\sin\theta_1}{\lambda}\right)^2 \\ \vdots \\ \left(\frac{2\sin\theta_n}{\lambda}\right)^2 \end{pmatrix} = \begin{pmatrix} k_1^2 & (2h_1+k_1)^2 & l_1^2 \\ & \vdots & \\ k_n^2 & (2h_n+k_n)^2 & l_n^2 \end{pmatrix} \begin{pmatrix} a^{-2} \\ m^{-2} \\ c^{-2} \end{pmatrix}. \quad (8)$$

We define the above matrices as $\mathbf{D} = \mathbf{AU}$. The lattice constant can be then obtained by solving the matrix equation

$$\mathbf{U} = (\mathbf{A}^T\mathbf{A})^{-1}(\mathbf{A}^T\mathbf{D}) \quad (9)$$

in any standard mathematical software package like Mathematica, Matlab, or Octave for a suitable set of at least three reflections. If there are more than three reflections, also an error can be estimated.

B. Calculation of relaxation

Stress causes the deformation of the lattice parameters, which leads to strain, i.e. the change of the lattice parameters. Assuming the X-axis along [1$\bar{2}$10], Y-axis along [10$\bar{1}$0] and Z-axis along [0001] direction, the relation between the stress σ and strain ε is given by Hooke's law which is for the wurtzite structure

$$\begin{pmatrix} \sigma_{xx} \\ \sigma_{yy} \\ \sigma_{zz} \\ \sigma_{yz} \\ \sigma_{zx} \\ \sigma_{xy} \end{pmatrix} = \begin{pmatrix} C_{11} & C_{12} & C_{13} & 0 & 0 & 0 \\ C_{12} & C_{11} & C_{13} & 0 & 0 & 0 \\ C_{13} & C_{13} & C_{33} & 0 & 0 & 0 \\ 0 & 0 & 0 & C_{44} & 0 & 0 \\ 0 & 0 & 0 & 0 & C_{44} & 0 \\ 0 & 0 & 0 & 0 & 0 & C_{66} \end{pmatrix} \times \begin{pmatrix} \varepsilon_{xx} \\ \varepsilon_{yy} \\ \varepsilon_{zz} \\ 2\varepsilon_{yz} \\ 2\varepsilon_{zx} \\ 2\varepsilon_{xy} \end{pmatrix} \quad (10)$$

C_{ij} are the elastic constant.

For (10$\bar{1}$0) m-plane oriented layers, the crystal is free along the growth direction. Thus there is no force, which means $\sigma_{yy} = 0$. Then, the relationship between the strain values in different directions can be reduced to:

$$0 = \sigma_{yy} = C_{12}\varepsilon_{xx} + C_{11}\varepsilon_{yy} + C_{13}\varepsilon_{zz}. \quad (11)$$

Since we have no shear stress, the strain values are given by the deformations of the lattice along a, m, and c as:

$$\varepsilon_{xx} = \frac{a - a^{0,AlGaN}}{a^{0,AlGaN}}, \quad (12a)$$

$$\varepsilon_{yy} = \frac{m - m^{0,AlGaN}}{m^{0,AlGaN}}, \quad (12b)$$

$$\varepsilon_{zz} = \frac{c - c^{0,AlGaN}}{c^{0,AlGaN}}. \quad (12c)$$

where a, m, and c are the experimentally obtained lattice parameters, and $a^{0,AlGaN}$, $m^{0,AlGaN}$, and $c^{0,AlGaN}$ are the unstrained lattice parameters. Assuming Vegard's law, the unstrained lattice parameters and the elastic constants are depending on the Al composition x and are expressed as:

$$a^{0,AlGaN} = x\,a^{AlN} + (1-x)\,a^{GaN}, \quad (13a)$$

$$m^{0,AlGaN} = x\,m^{AlN} + (1-x)\,m^{GaN}, \quad (13b)$$

$$c^{0,AlGaN} = x\,c^{AlN} + (1-x)\,c^{GaN}, \quad (13c)$$

$$C_{ij}^{0,AlGaN} = x\,C_{ij}^{AlN} + (1-x)\,C_{ij}^{GaN}. \quad (13d)$$

Now the Eq. (11) can be numerically solved by iterative calculation since it only depends on one variable x. Here we solve it by varying the Al content to minimize σ_{yy} (e.g. using Excel).

V. DISCUSSION

From solving Eq. (9) the lattice parameters were estimated as shown in Fig. 4. With increasing thickness, the lattice parameters got closer to the relaxed values for AlGaN with a composition of 19 % AlN, which is indicated in Fig. 4 by the dashed lines. Also, a and c are larger than the relaxed values and thus there is tensile strain in-plane of the surface. Consequently, m shrinks in the vertical direction to minimize the strain energy, as expected with the orthorhombic distortion of non-polar oriented wurtzite layers[8].

From these lattice parameters, the Al composition (Fig. 5a) at each thickness was calculated from minimizing Eq. (11). The Al composition was also estimated from measurements

parameter.pdf

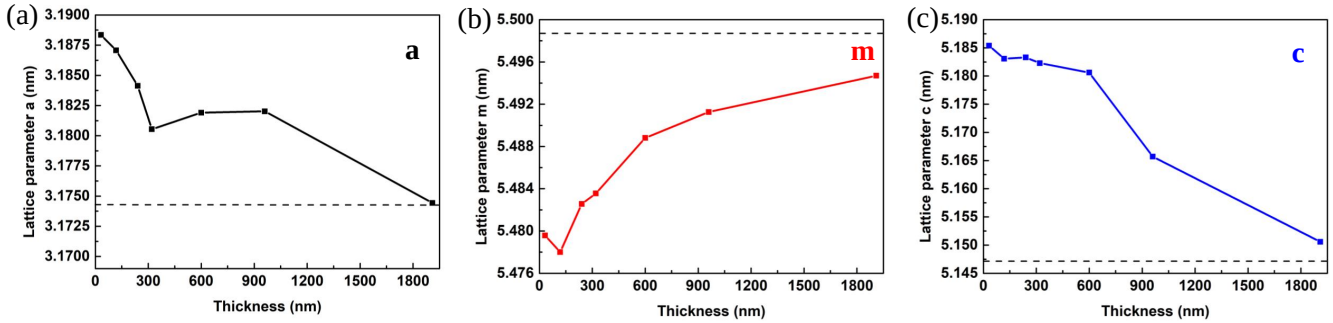


FIG. 4. Lattice parameter along the (a) a, (b) m, and (c) c axis with increasing thicknesses calculated from XRD. The dash lines indicate the relaxed values at 19 % Al-content.

value.pdf

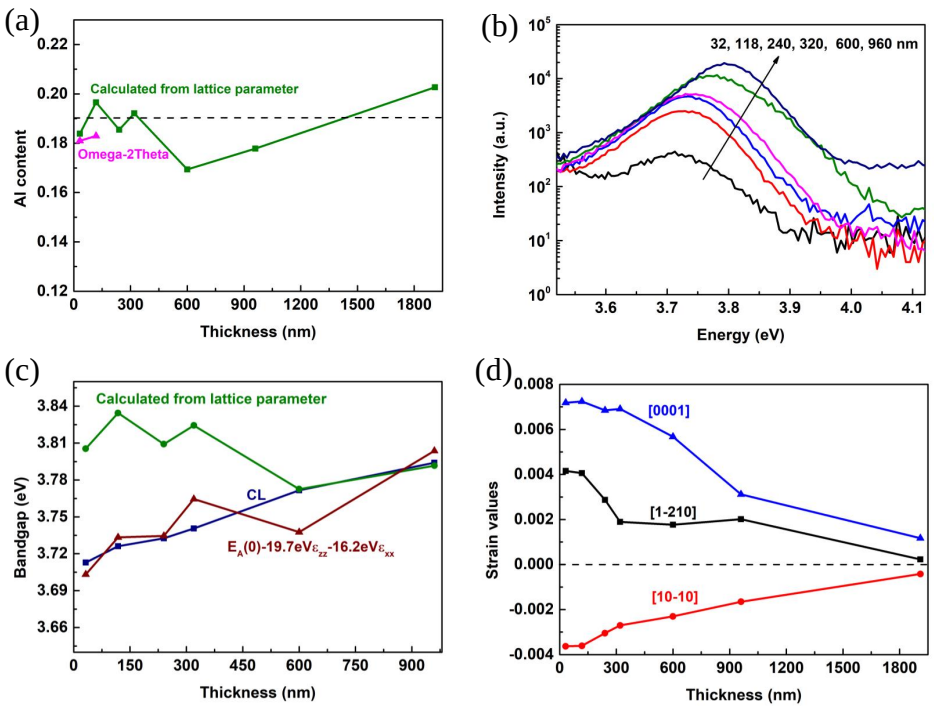


FIG. 5. (a) Al-content calculated from the lattice constants and simulations of $\omega-2\theta$ measurements using[14,15] (b) CL spectrum of AlGaN peak with different thicknesses (c) bandgap comparison between measured from CL, calculated from Al-content by lattice parameter determination, and our fitting (d) strain values of ε along $[1\bar{2}10]$, $[10\bar{1}0]$ and [0001] using the Al content from the lattice parameters.

of the symmetrical $10\bar{1}0$ and $30\bar{3}0$ reflections at 32 nm and 118 nm thickness and their simulations using the method of Oehler et al.[14,15] which assumes fully strained layers. Independently, the samples were measured with room-temperature cathodoluminescence (CL), as shown in Fig. 5b. It can be observed a tendency of a shift of AlGaN peak with thicknesses from 3.71 eV to 3.79 eV. The shift in the CL wavelength may be related to the effect of strain on the bandgap. The bandgap of relaxed AlGaN would be expected at $E_g(x) = 3.413(1-x)+6.2x-b_0x(1-x)$ assuming a bowing parameter of 0.8 eV[16] an AlN band gap of 6.2 eV[17,18] and 3.413 eV[19,20] for GaN at room temperature.

A. Effect of strain on the bandgap

We calculated the bandgap for unstrained AlGaN using the Al-content determined from the lattice constants. As shown in Fig. 5c, the deviation between the measured and calculated bandgap is decreasing with increasing thickness, i.e. decreasing strain. Comparable results have been reported only for GaN (0001) where the out-of-plane lattice constant was measured along [0001] direction from the 0002 reflection 2θ diffraction angle[21,22] even though the samples were strained in-plane. The out-of-plane strain along [0001] (ε_{zz}) can be converted to in-plane strain along $[1\bar{2}10]$ (ε_{xx}) for (0001) by

Hooke's law

$$\varepsilon_{xx} = -\frac{C_{33}}{2C_{13}}\varepsilon_{zz}. \tag{14}$$

For (0001) oriented epilayers, the uniform in-plane strain preserves the hexagonal symmetry of the basal plane, therefore, ε_{xx}=ε_{yy}.

The transition energies for (0001) orientation are a linear function of the applied strains[23]:

$$E_A = E_A(0) + (a_{cz} - D_1)\varepsilon_{zz} + (a_{ct} - D_2)\varepsilon_{\perp} - (D_3\varepsilon_{zz} + D_4\varepsilon_{\perp}) \tag{15a}$$

with $\varepsilon_{\perp}$=$\varepsilon_{xx}+\varepsilon_{yy}$, D_i are the valence-band deformation potentials, a_{cz} and a_{ct} are conduction-band deformation potentials. In the following we assume $a_{cz} - D_1 = -3.1\,\text{eV}$, $a_{ct} - D_2 = -11.2\,\text{eV}$, $D_3 = 8.2\,\text{eV}$, and $D_4 = -4.1\,\text{eV}$ from Ghosh et al.[24]. Then eq. (15a) can be written as:

$$E_A = E_A(0) - 11.3\,\text{eV}\varepsilon_{zz} - 14.2\,\text{eV}\varepsilon_{xx}. \tag{15b}$$

For (0001) orientation, the strain ε_{xx} can be substituted by ε_{zz} using eq. (14). Hence, E_A becomes a linear function of ε_{zz} as:

$$E_A = E_A(0) + 12.9\,\text{eV}\varepsilon_{zz}. \tag{15c}$$

Using the above values (from ref.[24]) for the different deformation potentials gives a linear coefficient of 12.9 eV for the A exciton. This is comparable to the reported value of $12\,eV$ by Amano et al.[22] and $15.4\,eV$ by Shikanai et al.[21].

For this publication, we assume a similar linear relation of the bandgap of the two in-plane strains:

$$E_A = E_A(0) + W_1\varepsilon_{zz} + W_2\varepsilon_{xx}. \tag{16}$$

with W_1 and W_2 the coefficients for ε_{zz} and ε_{xx}.

From the CL, we obtained a set of bandgaps of AlGaN, which is E_A. With the calculated bandgap obtained from Al-content ($E_A(0)$), and different strain along $[1\bar{2}10]$ and [0001], it is possible to obtain W_1 and W_2 by numerically solving the following matrix equation:

$$\begin{pmatrix} E_{A1} \\ \vdots \\ E_{An} \end{pmatrix} = \begin{pmatrix} E_A(0)_1 & \varepsilon_{zz1} & \varepsilon_{xx1} \\ & \vdots & \\ E_A(0)_n & \varepsilon_{zzn} & \varepsilon_{xxn} \end{pmatrix} \begin{pmatrix} 1 \\ W_1 \\ W_2 \end{pmatrix}. \tag{17}$$

As result, the bandgap dependence is:

$$E_A = E_A(0) - 19.7\,\text{eV}\varepsilon_{zz} - 16.2\,\text{eV}\varepsilon_{xx}. \tag{18}$$

Thus, we obtained linear coefficients of -19.7 eV for strain along [0001] and -16.2 eV for strain along $[1\bar{2}10]$. It is enlighting to compare the result of eq. (18) with eq. (15b) because experimentally only the cumulative effect of both strains can be measured in (0001) orientation.

However, we have to mention that the deformation potential for the valence band and conduction band for $(10\bar{1}0)$ still needs further calculation.

B. The anisotropic stress relaxation

The thick 1910 nm layer shows two distinct maxima for the $21\bar{3}0$ reflection, which suggests that the $\{10\bar{1}0\}\langle 1\bar{2}10\rangle$ slip system. The different change in reciprocal space along $[1\bar{2}10]$ and [0001] i.e. the two distinct maxima and the sudden broadening and deviation in q_x only appeared for the $21\bar{3}0$ reflection along $[1\bar{2}10]$ as well as the different surface morphology i.e. cracks only observed along $[1\bar{2}10]$ both suggest the anisotropic stress relaxation mechanisms along the two in-plane directions.

Along $[1\bar{2}10]$ direction, the $\{10\bar{1}0\}\langle 1\bar{2}10\rangle$ slip system accounts for the relaxation of tensile stress in the m-plane system[9]. Along [0001] direction, tensile stress is relaxed by the formation of cracks since there is no suitable slip system[25]. While the stress relaxation of m-plane AlGaN on GaN has been investigated focusing either on the prismatic slip[9] or cracking[25], the development of the relaxations are strongly connected with in-plane directions and is anisotropic.

The strain values along different directions (Fig. 5d) give further insight into the relaxation process. As expected from the lattice constants, the strain decreases with increasing thickness. Between 118 nm and 240 nm, the strain along $[1\bar{2}10]$ start to relax. It is already half relaxed after 240 nm and strongly relaxes with further thickness increase. In comparison, along [0001] it shows coherent growth to 320 nm, consistent with the observation that the first cracks just appeared in 320 nm AlGaN. Compared to the $[1\bar{2}10]$, the strain relaxation process along [0001] is slower with increasing thickness. Still half of the initial strain is left at 900 nm, and even the thickest layers at 1910 nm still show some strain. The result nicely illustrates that the stress relaxation is anisotropic on m-plane and it is easier to relax stress via slip compared to cracking.

C. Critical thickness along the different directions

For $21\bar{3}0$ reflection, it broadens strongly in XRD-RSMs (Fig.1) for AlGaN between 118 nm and 240 nm along $[1\bar{2}10]$, correlating with the onset of large undulations in the white light interference microscopy images parallel to [0001] observed in 240 nm sample. At this thickness, the in-plane strain along $[1\bar{2}10]$ strongly decreases (Fig. 5d). Hence, we obtained the occurrence of stress relaxation along $[1\bar{2}10]$ in our 19% AlGaN is between 118 nm and 240 nm.

For the estimation of the critical thickness (h_c) for stress relaxation along $[1\bar{2}10]$, the Matthews and Blakeslee (MB) model is adopted, given in eq. (19). The MB theory predicts h_c for the MD formation. It is based on energy equilibrium between the formation of a MD with Burgers vector at the interface of the strained epilayer on a substrate with different lattice parameter through slip.[26]

$$f = \frac{\mathbf{b}}{h_c}\frac{1-\nu\cos^2\alpha}{4\pi(1+\nu)\cos\lambda}\left(\ln\frac{h_c}{|\mathbf{b}|}+1\right) \tag{19}$$

Where f is the lattice mismatch between AlGaN and GaN, ν is the Poisson's ratio, $\mathbf{b}$ is the Burgers vector. The angular

factors λ and α depend on the slip system: The angle λ is between the Burgers vector **b** and the interface. The angle α is between the dislocation line and the Burgers vector.

The Poisson's ratio for (0001) GaN is defined as $\frac{\varepsilon_{xx}}{\varepsilon_{zz}} = -\frac{C_{33}}{2C_{13}} = -\frac{1-\nu}{2\nu}$, therefore, $\nu = 0.23$. While for m-plane GaN, there are two independent Poisson ratios, $\nu_{am} = \frac{C_{12}C_{33}-C_{13}^2}{C_{11}C_{33}-C_{13}^2} = 0.32$ and $\nu_{cm} = \frac{C_{13}}{C_{11}+C_{12}} = 0.21$ (appendix). For slip along $[1\bar{2}10]$, the slip system is approximately 60° inclined. Therefore, ν_{am} should be adopted in MB model for h_c. While for the [0001], the only slip plane would be the (0001) plane which is 90° to the growth plane. The equation of MB model cannot produce a solution as the denominator becomes zero and thus the MB model cannot be applied for crack formation.

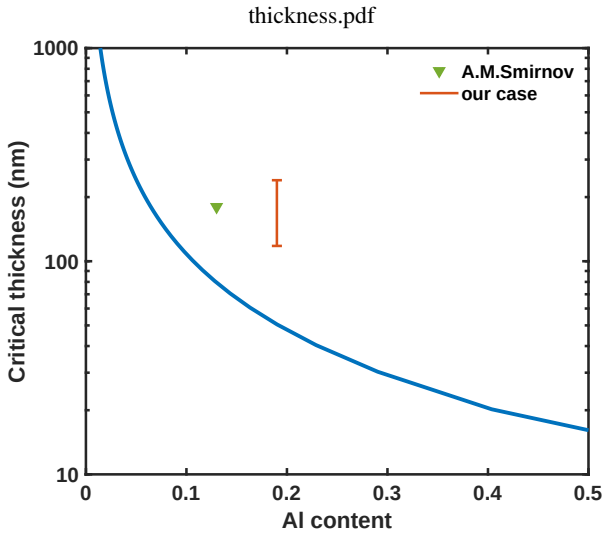


FIG. 6. Comparison of the h_c estimated for $Al_xGa_{1-x}N$/GaN system via $\{10\bar{1}0\}\langle 1\bar{2}10\rangle$ slip system with the experiment results.

Fig. 6 compares the calculated h_c estimated from $\{10\bar{1}0\}\langle 1\bar{2}10\rangle$ slip system with the experimental results, here $\mathbf{b} = a_{AlGaN}$, $a(x) = a_{AlGaN}$, $f = \frac{a_{GaN}-a_{Al_xGa_{1-x}N}}{a_{GaN}}$, $\cos\lambda = \frac{1}{2}$, $\sin\alpha = 1$. The blue solid line correspond to the h_c using $\nu = 0.32$. The green triangle represents the h_c reported by A. M. Smirnov et al.[9] for 13% AlGaN, the slip already happened at 180 nm. The red bar represents our case that found the onset of slip for 19% AlGaN between 118 nm to 240 nm.

Due to the lack of a suitable slip system for [0001] direction[25] and the orthogonality of the slip system of $\{10\bar{1}0\}\langle 1\bar{2}10\rangle$ and the c-plane, even if the stress is fully relaxed along $[1\bar{2}10]$, the stress along [0001] would remain almost the same. Indeed, this can be seen in Fig. 5d up to 320 nm, when already half the strain along $[1\bar{2}10]$ was relaxed. Consequently, the first cracks along $[1\bar{2}10]$ appeared at 320 nm AlGaN and their numbers increased with increasing AlGaN thickness. Thus, we found for 19% AlGaN a critical thickness for cracking between 240 nm and 320 nm, which is much higher than the values of 120-150 nm for 17% AlGaN from Young et al.[27] and our results are more similar to $(11\bar{2}2)$ which showed no cracking for 15% up to 250 nm AlGaN[25].

TABLE I. Elastic constant, lattice constant, bandgap and bowing parameter of AlN and GaN used in the calculation.

Materials	C_{11}	C_{12}	C_{13}	C_{33}	a_0 (nm)	c_0 (nm)	E_g (eV)	Bowing (eV)
AlN	384	137	109	386	0.311197	0.498089	6.2	0.8
GaN	362	137	105	358	0.31894	0.518614	3.413	-

The much earlier onset of cracking reported by Young et al. for $(10\bar{1}0)$ might be related to their surface treatment, since both $(10\bar{1}0)$ should first relax stress via slip along $[1\bar{2}10]$ and thus show a later onset of cracking. Instead, a value of 120-150 nm would be similar to the (0001) orientation, where the onset of cracking of 17% AlGaN was reported at 110 nm[28].

VI. CONCLUSION

We have systematically studied the development of strain of 19 % $(10\bar{1}0)$ AlGaN layers on GaN. To assess the strain state, we developed a relatively simple method to calculate the lattice parameters and Al content from XRD measurement for m-plane AlGaN. The stress relaxation for m-plane AlGaN/GaN heterostructure is anisotropic along the in-plane directions. The stress along $[1\bar{2}10]$ is relaxed first by prismatic plane slip for layers thicker than 118 nm while the stress along [0001] relaxes by cracks formation for layers thicker than 240 nm due to the lack of a slip system. Furthermore, stress relaxation progresses much fast with an increasing thickness along $[1\bar{2}10]$ direction. From the shift of the CL emission, we could show that the bandgap decreases with increasing tensile strain no matter if along [0001] or $[1\bar{2}10]$. From this, we obtained the relation of the bandgap energy on m-plane with the strain $E_A = E_0 - 19.7\,\mathrm{eV}\varepsilon_{[0001]} - 16.2\,\mathrm{eV}\varepsilon_{[1\bar{2}10]}$.

ACKNOWLEDGEMENT

This work was supported, in part, by JSPS KAKENHI Grant Number JP21K04138. Yingying Lin acknowledges the China Scholarship Council file NO.20210805179.

Appendix A: Poisson ratios of GaN

According to the definition of the Poisson's ratio, it is the negative ratio between transverse strain (ε_t) and longitudinal strain (ε_l) in the elastic deformation. Theoretically, the value of Poisson's ratio is ranging between -1 and 0.5. For most materials, the Poisson's ratio is between 0 and 0.5. In anisotropic materials, the Poisson ratio can exceed 0.5 along certain directions.

For m-plane GaN, the deformation is orthotropic and we have three different Poisson ratios. To obtain them, the

Hooke's law can be expressed in matrix form as eq. (A1)

$$\begin{pmatrix} \varepsilon_{xx} \\ \varepsilon_{yy} \\ \varepsilon_{zz} \\ 2\varepsilon_{yz} \\ 2\varepsilon_{zx} \\ 2\varepsilon_{xy} \end{pmatrix} = \begin{pmatrix} \frac{1}{E_x} & -\frac{\nu_{yx}}{E_y} & -\frac{\nu_{zx}}{E_z} & 0 & 0 & 0 \\ -\frac{\nu_{xy}}{E_x} & \frac{1}{E_y} & -\frac{\nu_{zy}}{E_z} & 0 & 0 & 0 \\ -\frac{\nu_{xz}}{E_x} & -\frac{\nu_{yz}}{E_y} & \frac{1}{E_z} & 0 & 0 & 0 \\ 0 & 0 & 0 & \frac{1}{G_{yz}} & 0 & 0 \\ 0 & 0 & 0 & 0 & \frac{1}{G_{zx}} & 0 \\ 0 & 0 & 0 & 0 & 0 & \frac{1}{G_{xy}} \end{pmatrix} \times \begin{pmatrix} \sigma_{xx} \\ \sigma_{yy} \\ \sigma_{zz} \\ \sigma_{yz} \\ \sigma_{zx} \\ \sigma_{xy} \end{pmatrix} \tag{A1}$$

E_i is the Young's modulus along axis i, G_{ij} is the shear modulus in direction j on the plane whose normal is in direction i, ν_{ij} is the Poisson's ratio when a strain in direction j when an strain is applied in direction i.

The 6×6 matrix of eq. (A1) is the inverse of eq. (10). Thus, we can invert eq. (10) the Poisson's ratio along different direction for m-plane GaN can be obtained. For our case we need the two Poisson ratios $\nu_{xy} = \nu_{am}$ and $\nu_{zy} = \nu_{cm}$. The can be directly compared from the matrices using the coefficients from Tab. A:

$$\nu_{xy} = \frac{\frac{\nu_{xy}}{E_x}}{\frac{1}{E_x}} = \frac{C_{12}C_{33} - C_{13}^2}{C_{11}C_{33} - C_{13}^2} = 0.32 \tag{A2}$$

$$\nu_{zy} = \frac{\frac{\nu_{zy}}{E_z}}{\frac{1}{E_z}} = \frac{C_{13}}{C_{11} + C_{12}} = 0.21. \tag{A3}$$

[1] A. E. Romanov, E. C. Young, F. Wu, A. Tyagi, C. S. Gallinat, S. Nakamura, S. P. DenBaars, J. S. Speck, Basal plane misfit dislocations and stress relaxation in III-nitride semipolar heteroepitaxy, J. Appl. Phys. 109 (10) (2011) 103522 (2011). doi:10.1063/1.3590141.

[2] A. E. Romanov, T. J. Baker, S. Nakamura, J. S. Speck, E. U. Group, Strain-induced polarization in wurtzite iii-nitride semipolar layers, J. Appl. Phys. 100 (2) (2006) 023522 (2006). doi:10.1063/1.2218385.

[3] S. Einfeldt, H. Heinke, V. Kirchner, D. Hommel, Strain relaxation in AlGaN/GaN superlattices grown on GaN, J. Appl. Phys. 89 (4) (2001) 2160–2167 (2001). doi:10.1063/1.1342020.

[4] S. R. Lee, D. D. Koleske, K. C. Cross, J. A. Floro, K. E. Waldrip, A. T. Wise, S. Mahajan, In situ measurements of the critical thickness for strain relaxation in AlGaN/GaN heterostructures, Appl. Phys. Lett. 85 (25) (2004) 6164–6166 (2004). doi:10.1063/1.1840111.

[5] J. Floro, D. Follstaedt, P. Provencio, S. Hearne, S. Lee, Misfit dislocation formation in the AlGaN/GaN heterointerface, J. Appl. Phys. 96 (12) (2004) 7087–7094 (2004). doi:10.1063/1.1812361.

[6] G. Ju, M. Tabuchi, Y. Takeda, H. Amano, Role of threading dislocations in strain relaxation during gainn growth monitored by real-time x-ray reflectivity, Applied Physics Letters 110 (26) (2017) 262105 (2017).

[7] S. Srinivasan, L. Geng, R. Liu, F. Ponce, Y. Narukawa, S. Tanaka, Slip systems and misfit dislocations in ingan epilayers, Applied Physics Letters 83 (25) (2003) 5187–5189 (2003).

[8] M. R. Laskar, T. Ganguli, A. Rahman, A. Mukherjee, N. Hatui, M. Gokhale, A. Bhattacharya, Distorted wurtzite unit cells: Determination of lattice parameters of nonpolar a-plane algan and estimation of solid phase al content, Journal of Applied Physics 109 (1) (2011) 013107 (2011).

[9] A. Smirnov, E. Young, V. Bougrov, J. Speck, A. Romanov, Critical thickness for the formation of misfit dislocations originating from prismatic slip in semipolar and nonpolar III-nitride heterostructures, APL Materials 4 (1) (2016) 016105 (2016). doi:10.1063/1.4939907.

[10] A. Tanaka, Y. Ando, K. Nagamatsu, M. Deki, H. Cheong, B. Ousmane, M. Kushimoto, S. Nitta, Y. Honda, H. Amano, m-plane gan schottky barrier diodes fabricated with movpe layer on several off-angle m-plane gan substrates, physica status solidi (a) 215 (9) (2018) 1700645 (2018).

[11] S. Yoshida, T. Yokogawa, Y. Imai, S. Kimura, O. Sakata, Evidence of lattice tilt and slip in m-plane ingan/gan heterostructure, Applied Physics Letters 99 (13) (2011) 131909 (2011).

[12] M. Fujikane, T. Yokogawa, S. Nagao, R. Nowak, Yield shear stress dependence on nanoindentation strain rate in bulk gan crystal, physica status solidi c 8 (2) (2011) 429–431 (2011).

[13] M. Frentrup, N. Hatui, T. Wernicke, J. Stellmach, A. Bhattacharya, M. Kneissl, Determination of lattice parameters, strain state and composition in semipolar iii-nitrides using high resolution x-ray diffraction, J. Appl. Phys. 114 (21) (2013) 213509 (2013). doi:10.1063/1.4834521.

[14] F. Oehler, M. E. Vickers, M. J. Kappers, R. A. Oliver, Alloy content determination of fully strained and partially relaxed semi-polar group III-nitrides by X-ray diffraction, J. Appl. Phys. 114 (5) (2013) 053520 (2013). doi:10.1063/1.4817422.

[15] F. Oehler, M. E. Vickers, M. J. Kappers, R. A. Oliver, Erratum: Alloy content determination of fully strained and partially relaxed semi-polar group III-nitrides by X-ray diffraction; [j. appl. phys. 114, 053520 (2013)], J. Appl. Phys. 114 (21) 219901. doi:10.1063/1.4845955.

[16] Y. Koide, H. Itoh, M. Khan, K. Hiramatu, N. Sawaki, I. Akasaki, Energy band-gap bowing parameter in an al x ga1- x n alloy, Journal of applied physics 61 (9) (1987) 4540–4543 (1987).

[17] W. Yim, E. Stofko, P. Zanzucchi, J. Pankove, M. Ettenberg, S. Gilbert, Epitaxially grown aln and its optical band gap, Journal of Applied Physics 44 (1) (1973) 292–296 (1973).

[18] P. Perry, R. Rutz, The optical absorption edge of single-crystal aln prepared by a close-spaced vapor process, Applied Physics Letters 33 (4) (1978) 319–321 (1978).

[19] R. Dingle, D. Sell, S. Stokowski, M. Ilegems, Absorption, reflectance, and luminescence of gan epitaxial layers, Physical Review B 4 (4) (1971) 1211 (1971).

[20] B. Monemar, Fundamental energy gap of gan from photoluminescence excitation spectra, Physical Review B 10 (2) (1974) 676 (1974).

[21] A. Shikanai, T. Azuhata, T. Sota, S. Chichibu, A. Kuramata, K. Horino, S. Nakamura, Biaxial strain dependence of exciton resonance energies in wurtzite GaN, J. Appl. Phys. 81 (1) (1997) 417–424 (1997). doi:10.1063/1.364074.

[22] H. Amano, K. Hiramatsu, I. Akasaki, Heteroepitaxial growth and the effect of strain on the luminescent properties of gan films on (11 20) and (0001) sapphire substrates, Japanese journal of applied physics 27 (8A) (1988) L1384 (1988).

[23] Q. Yan, P. Rinke, M. Scheffler, C. G. Van de Walle, Strain effects in group-iii nitrides: Deformation potentials for aln, gan, and inn, Applied Physics Letters 95 (12) (2009) 121111 (2009).

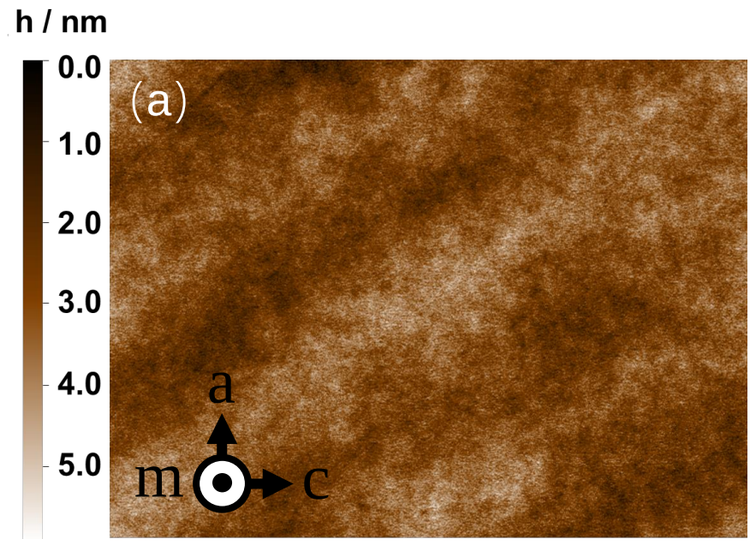
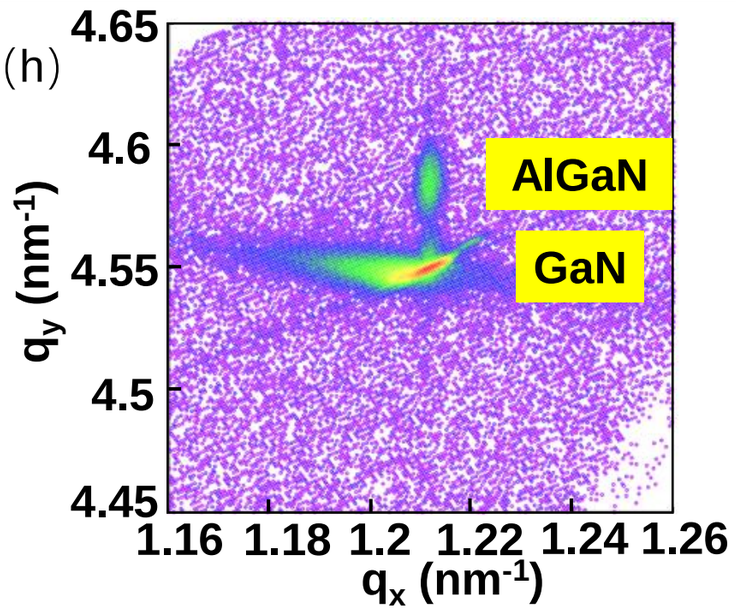
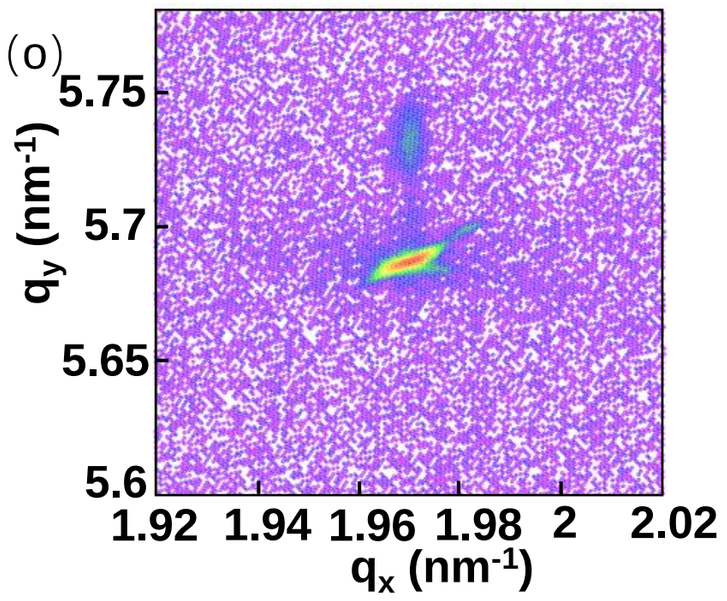
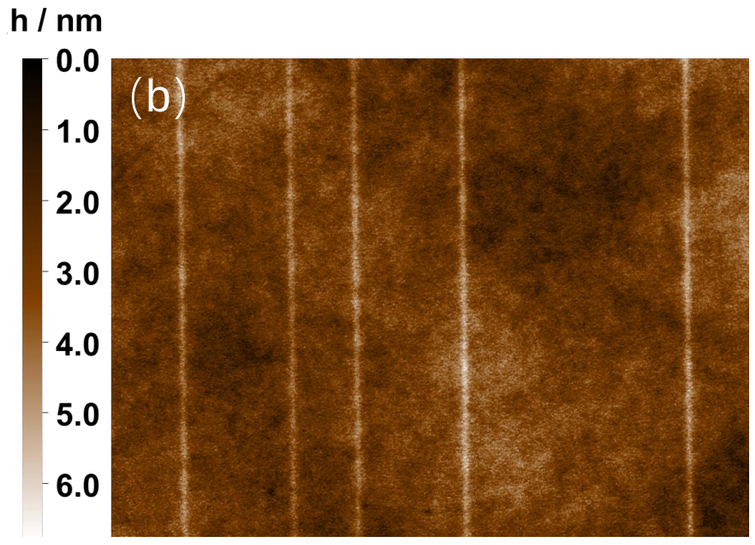
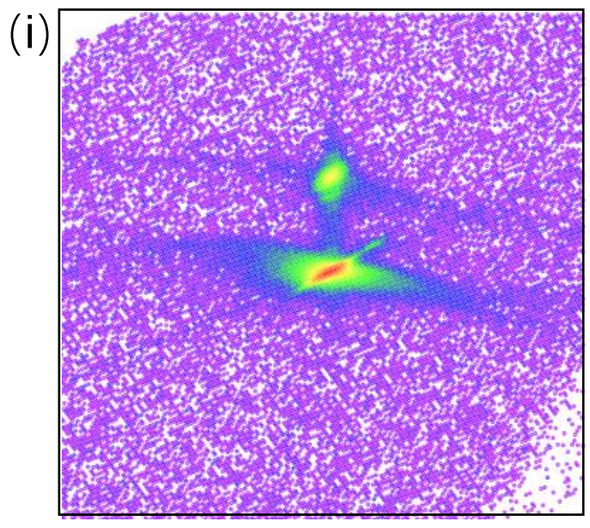
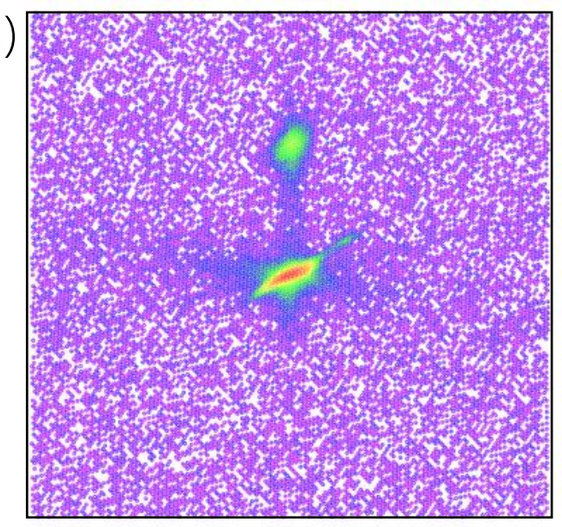
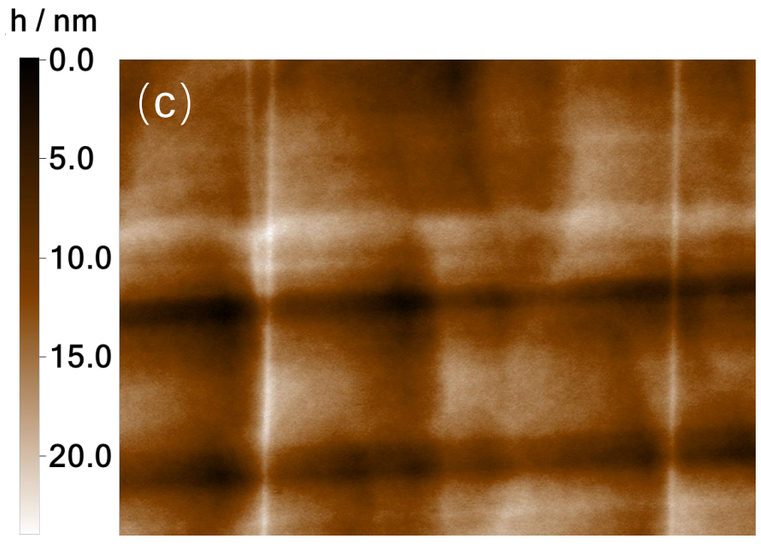
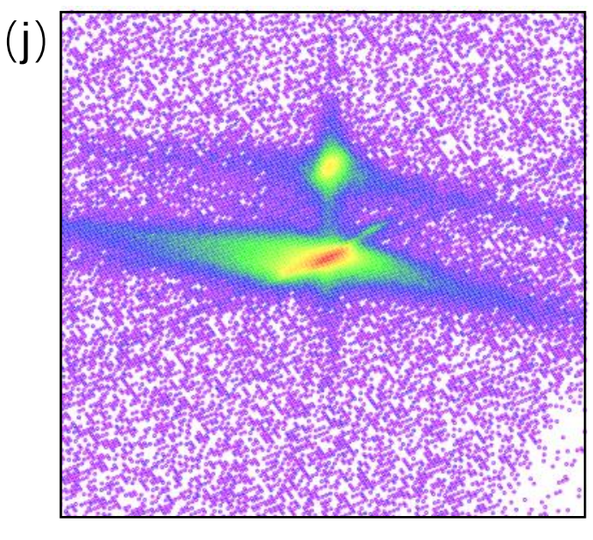
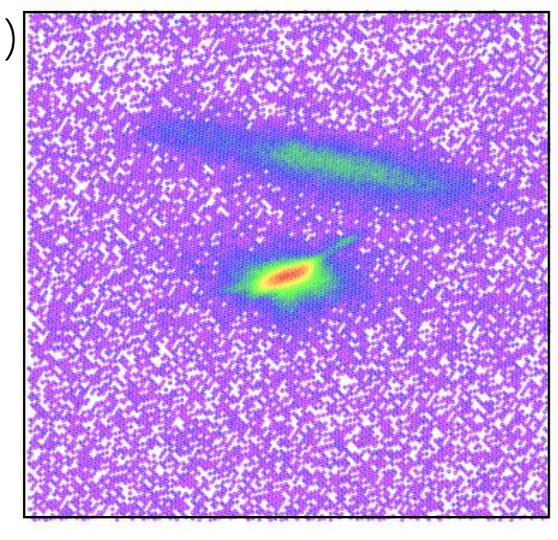
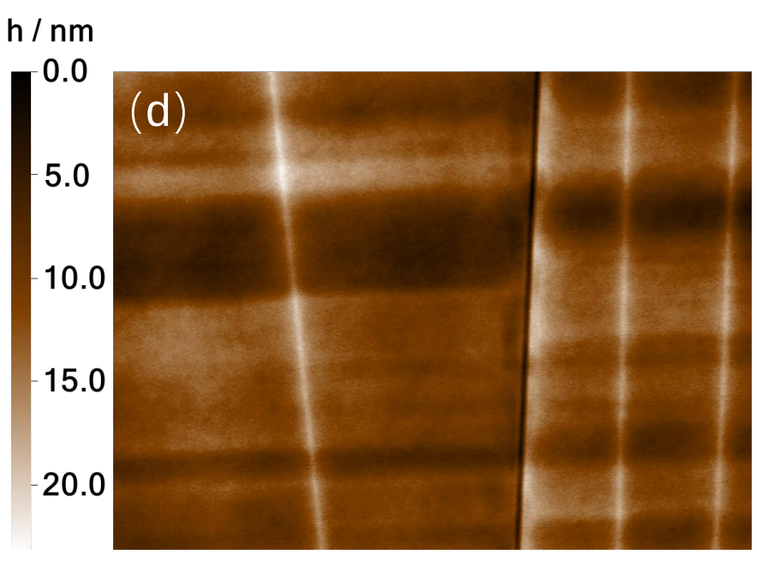
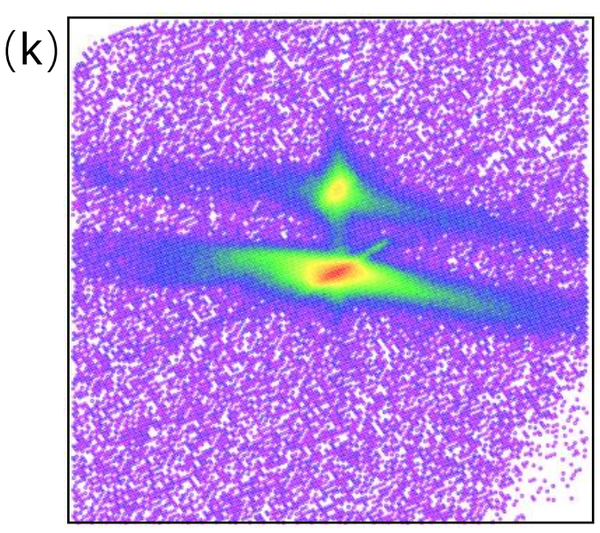
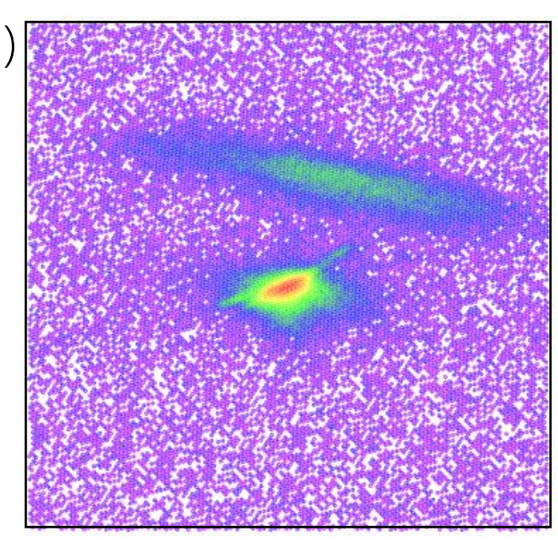
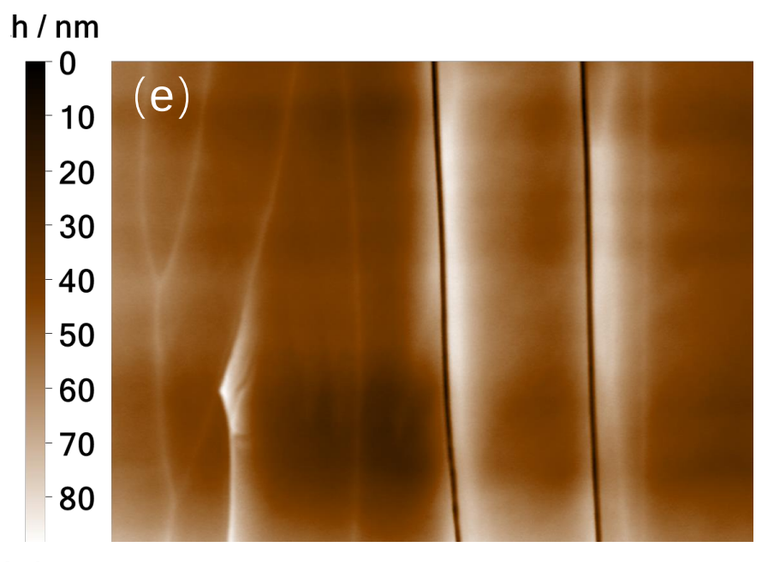
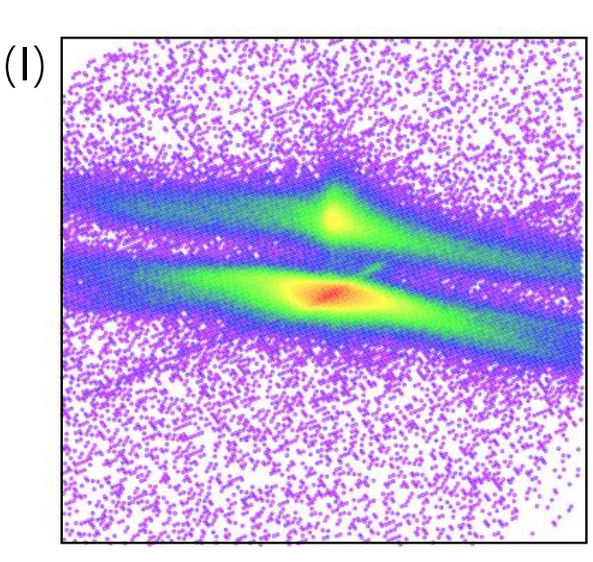
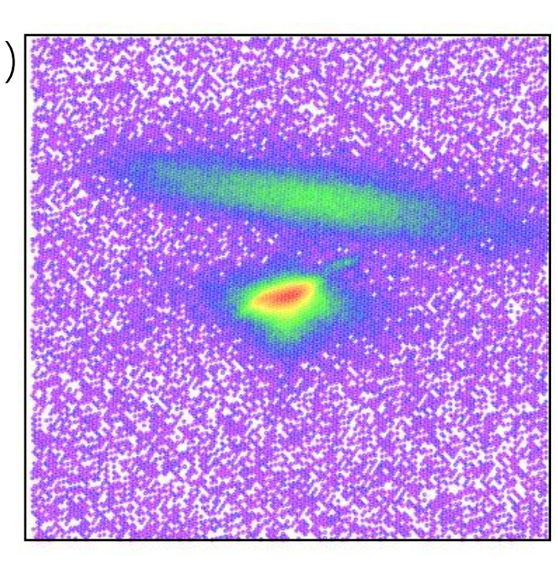
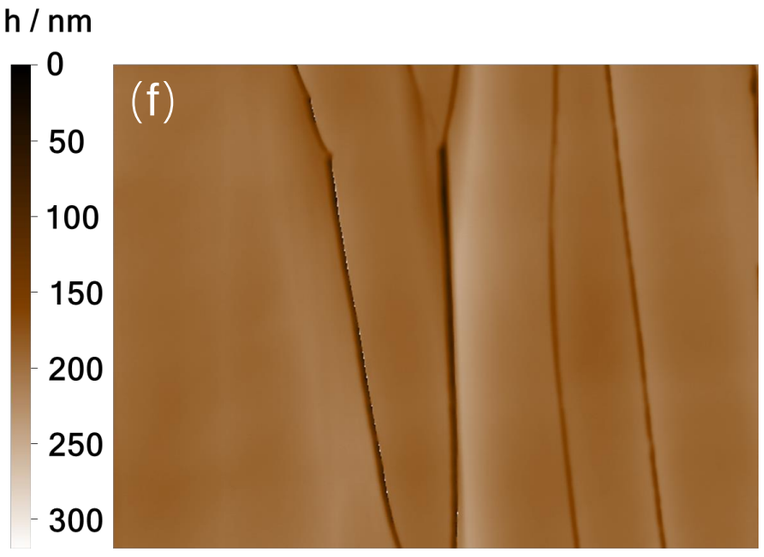
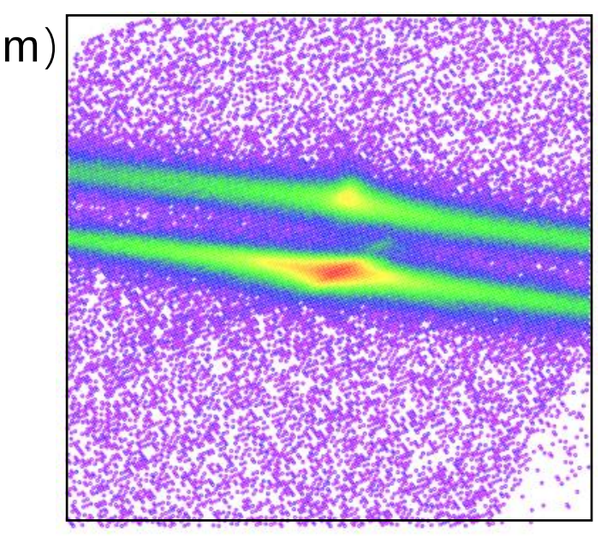
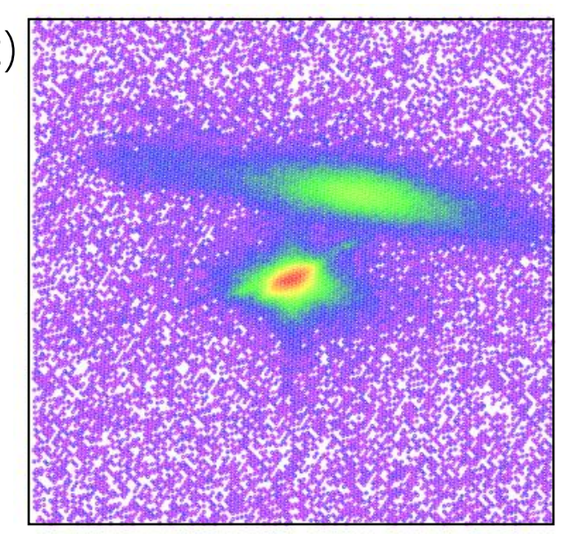
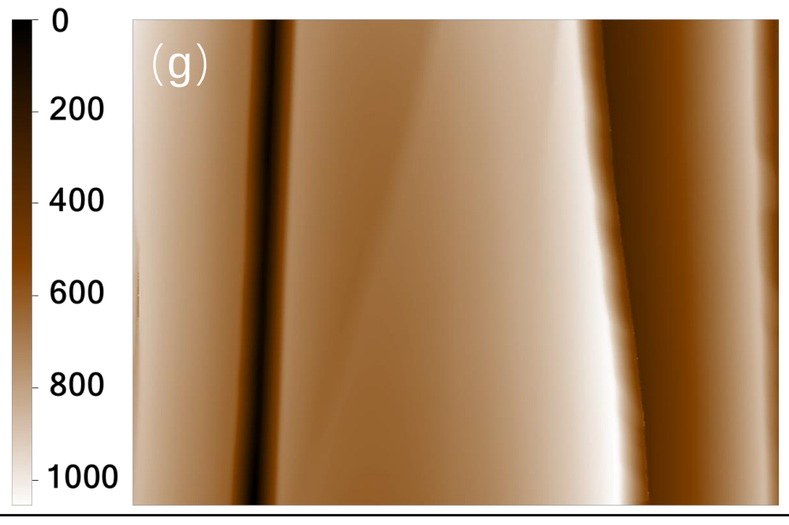
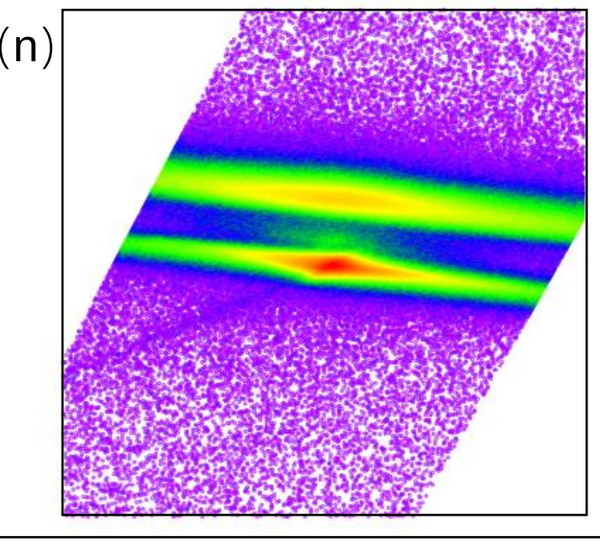
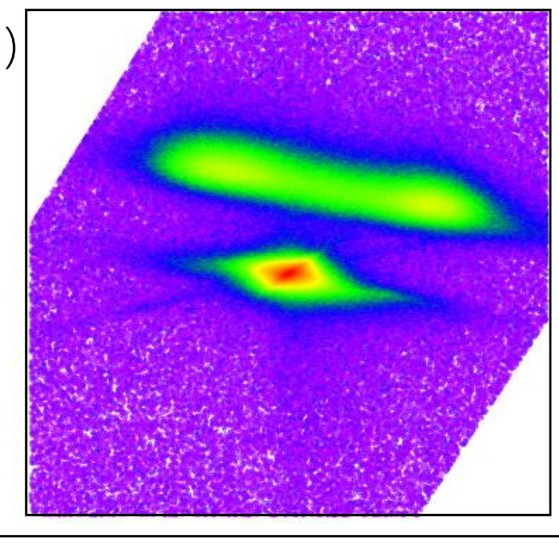
[24] S. Ghosh, P. Waltereit, O. Brandt, H. Grahn, K. Ploog, Electronic band structure of wurtzite gan under biaxial strain in the m plane investigated with photoreflectance spectroscopy, Physical Review B 65 (7) (2002) 075202 (2002).

[25] E. C. Young, F. Wu, A. E. Romanov, A. Tyagi, C. S. Gallinat, S. P. DenBaars, S. Nakamura, J. S. Speck, Lattice tilt and misfit dislocations in $(11\bar{2}2)$ semipolar GaN heteroepitaxy, Applied physics express 3 (1) (2010) 011004 (2010). doi:10.1143/APEX.3.011004.

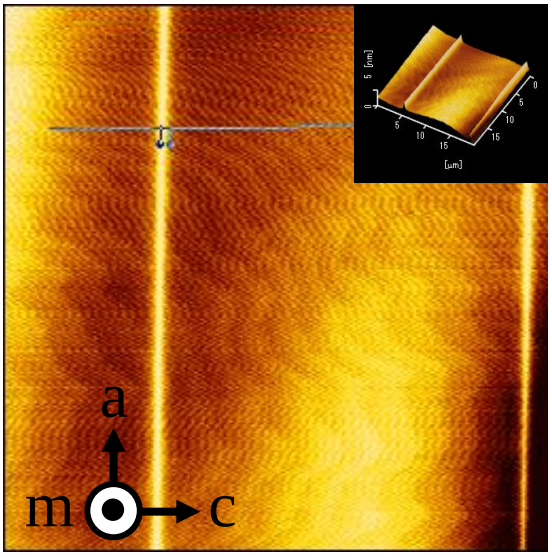
[26] J. Matthews, A. Blakeslee, Defects in epitaxial multilayers: I. misfit dislocations, Journal of Crystal growth 27 (1974) 118–125 (1974).

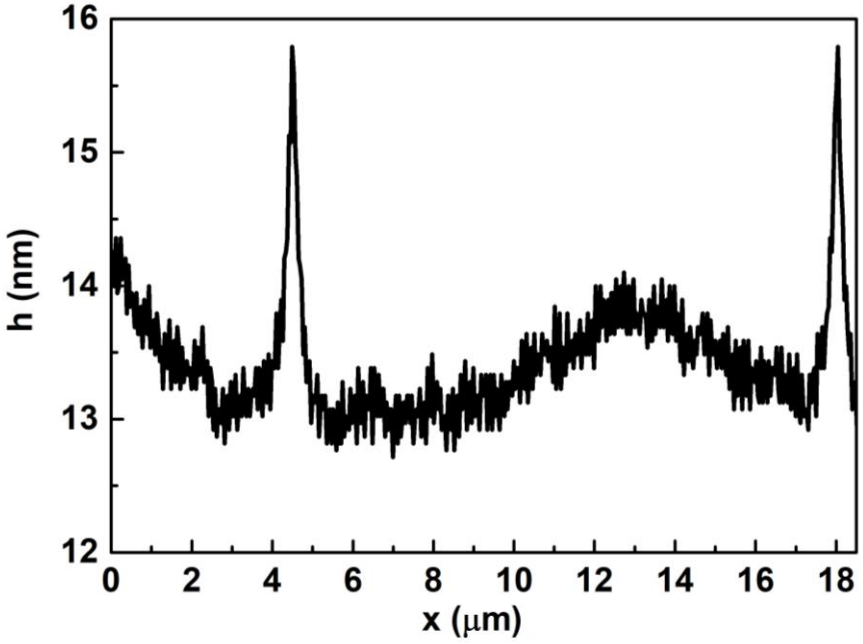
[27] E. C. Young, A. E. Romanov, C. S. Gallinat, A. Hirai, G. E. Beltz, J. S. Speck, Anisotropy of tensile stresses and cracking in nonbasal plane AlGaN/GaN heterostructures, Applied Physics Letters 96 (4) (2010) 041913 (2010). doi:10.1063/1.3276561.

[28] S. Hearne, J. Han, S. Lee, J. Floro, D. Follstaedt, E. Chason, I. Tsong, Brittle-ductile relaxation kinetics of strained algan/gan heterostructures, Applied Physics Letters 76 (12) (2000) 1534–1536 (2000).

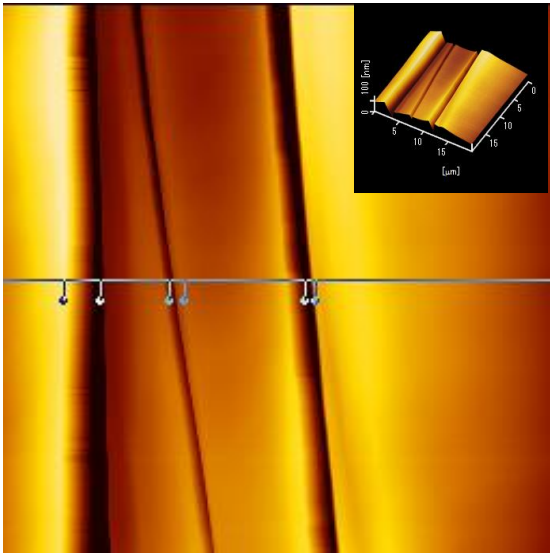
AlGaN thickness	Optical interferometry	20-21 reflection λ // [0001]	21-30 reflection λ // [1-210]
32 nm			
118 nm			
240 nm			
320 nm			
600 nm			
960 nm			
1910 nm			

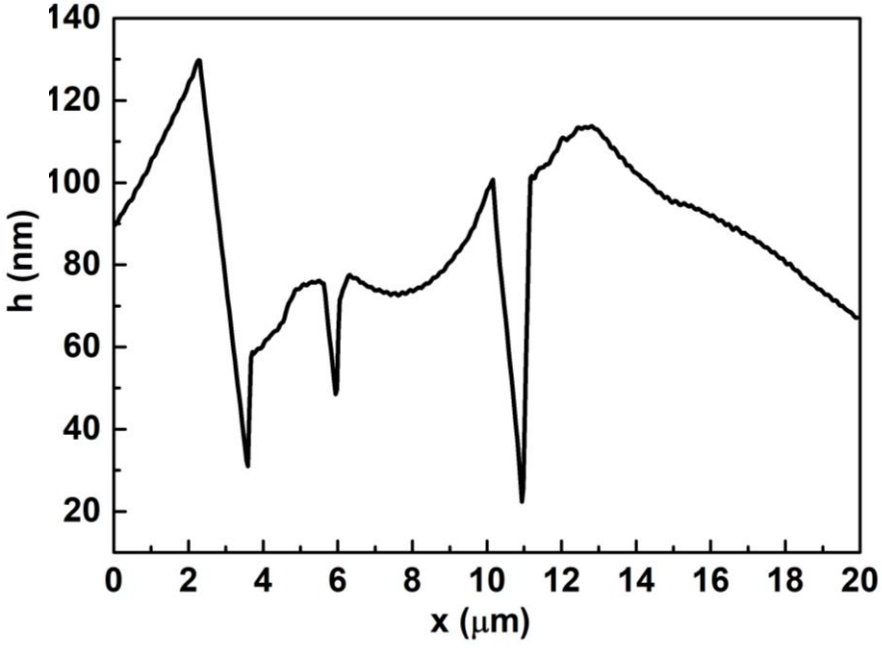
(a)

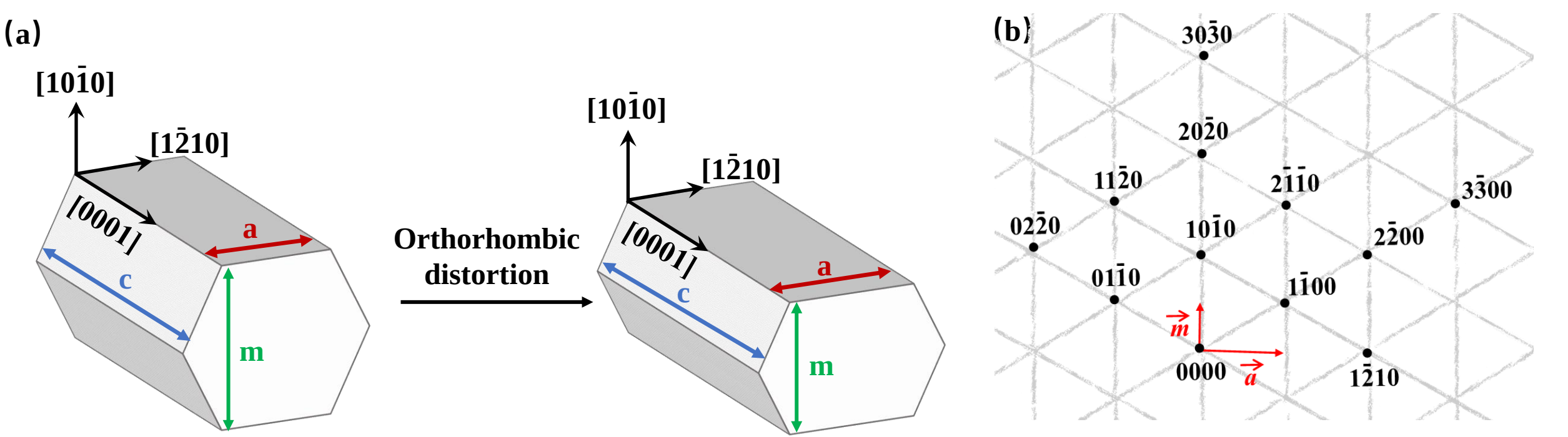

a
m
c

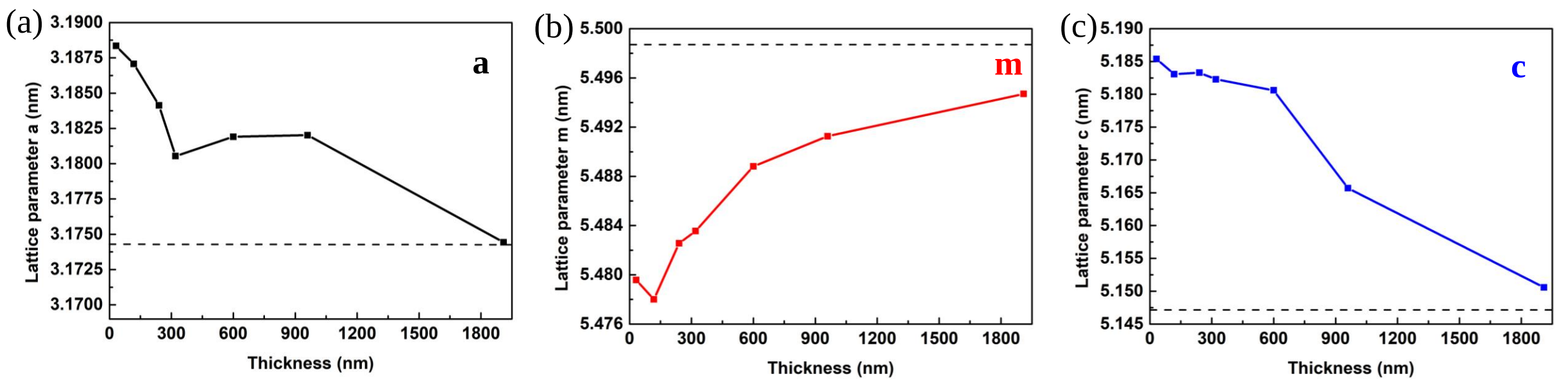

h (nm)
x (μm)
16
15
14
13
12
0
2
4
6
8
10
12
14
16
18

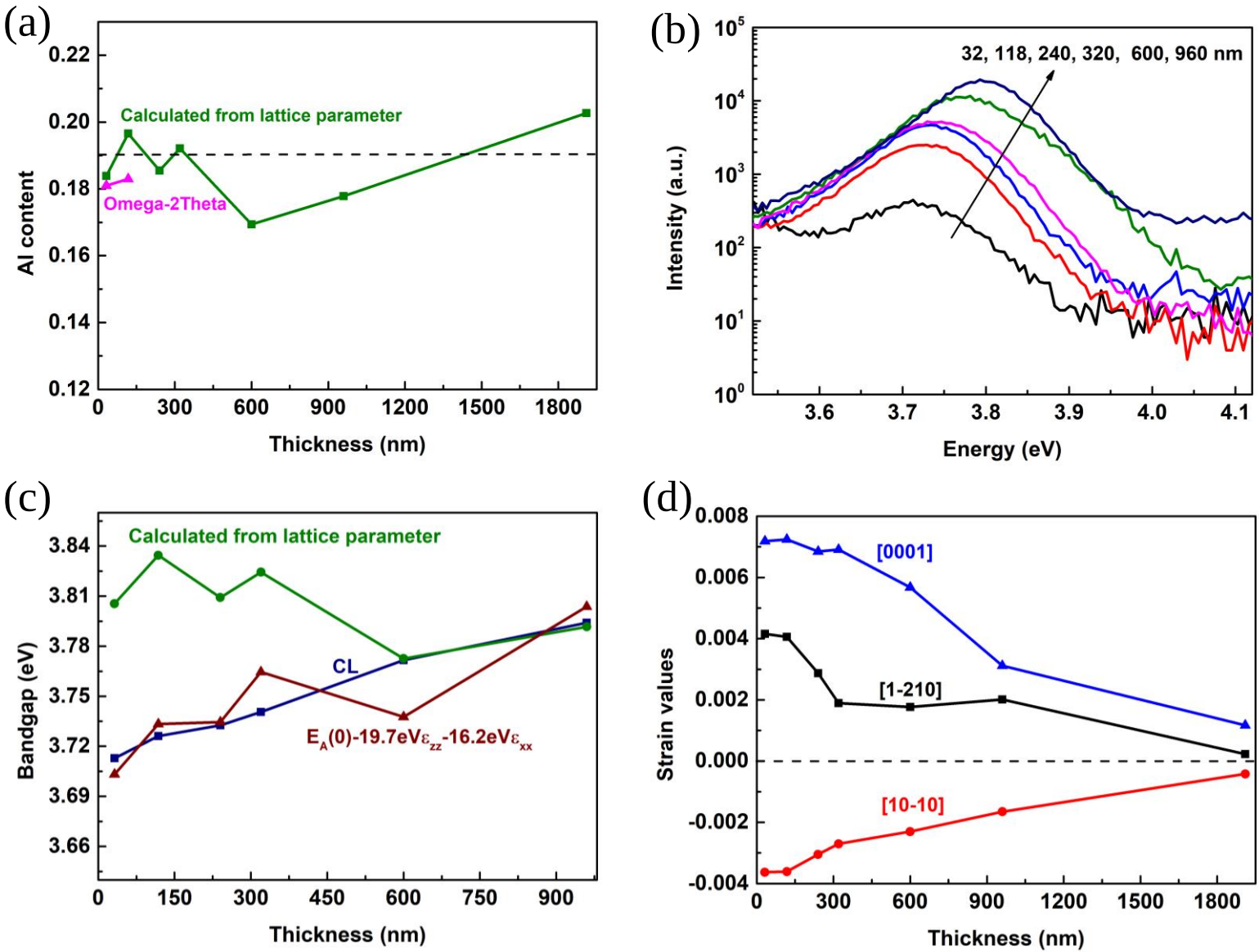
(b)

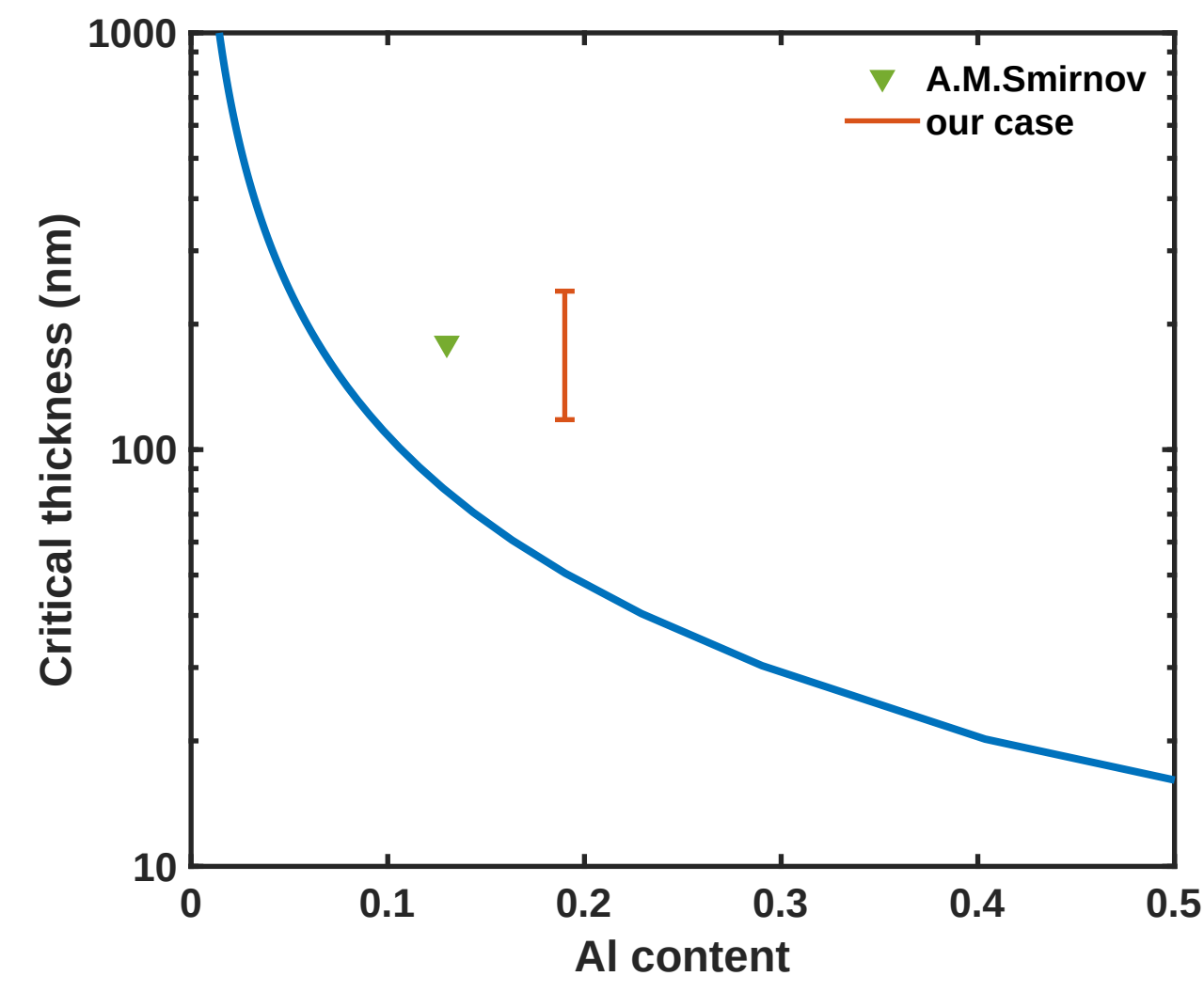



h (nm)
x (μm)
140
120
100
80
60
40
20
0
2
4
6
8
10
12
14
16
18
20


(a)
[10$\bar{1}$0]
[1$\bar{2}$10]
[0001]
a
c
m
Orthorhombic distortion
[10$\bar{1}$0]
[1$\bar{2}$10]
[0001]
a
c
m
(b)
30$\bar{3}$0
20$\bar{2}$0
11$\bar{2}$0
2$\bar{1}\bar{1}$0
3$\bar{3}$00
02$\bar{2}$0
10$\bar{1}$0
2$\bar{2}$00
01$\bar{1}$0
1$\bar{1}$00
$\vec{m}$
0000
$\vec{a}$
1$\bar{2}$10


(a)
a
Lattice parameter a (nm)
3.1900
3.1875
3.1850
3.1825
3.1800
3.1775
3.1750
3.1725
3.1700
0
300
600
900
1200
1500
1800
Thickness (nm)
(b)
m
Lattice parameter m (nm)
5.500
5.496
5.492
5.488
5.484
5.480
5.476
0
300
600
900
1200
1500
1800
Thickness (nm)
(c)
c
Lattice parameter c (nm)
5.190
5.185
5.180
5.175
5.170
5.165
5.160
5.155
5.150
5.145
0
300
600
900
1200
1500
1800
Thickness (nm)


(a)
Calculated from lattice parameter
Omega-2Theta
Al content
Thickness (nm)
(b)
32, 118, 240, 320, 600, 960 nm
Intensity (a.u.)
Energy (eV)
(c)
Calculated from lattice parameter
CL
$E_A(0)-19.7eV\varepsilon_{zz}-16.2eV\varepsilon_{xx}$
Bandgap (eV)
Thickness (nm)
(d)
[0001]
[1-210]
[10-10]
Strain values
Thickness (nm)


1000
100
10
Critical thickness (nm)
0
0.1
0.2
0.3
0.4
0.5
Al content
A.M.Smirnov
our case